INTERNATIONAL SOCIETY FOR SOIL MECHANICS AND GEOTECHNICAL ENGINEERING



This paper was downloaded from the Online Library of the International Society for Soil Mechanics and Geotechnical Engineering (ISSMGE). The library is available here:

https://www.issmge.org/publications/online-library

This is an open-access database that archives thousands of papers published under the Auspices of the ISSMGE and maintained by the Innovation and Development Committee of ISSMGE.

The paper was published in the proceedings of the 7th International Conference on Earthquake Geotechnical Engineering and was edited by Francesco Silvestri, Nicola Moraci and Susanna Antonielli. The conference was held in Rome, Italy, 17 - 20 June 2019.

Energy-based Newmark method for slope displacement without need of acceleration time-history

T. Kokusho

Chuo University, Tokyo, Japan

ABSTRACT: Nonlinear numerical analyses are conducted wherein the Newmark-type slope model is shaken by SH wave propagating underneath. Earthquake energy for slope sliding as the energy difference between upward and downward waves is confirmed to balance with other energies associated with slope sliding. The residual slope displacements δ_r are uniquely correlated with the earthquake energy despite the difference in earthquake motions, indicating that δ_r can be readily evaluated without using acceleration time-histories. The evaluation procedure has been developed using the analytical results and empirical formulas on input wave energies. An example study for slope displacements of varying hypocenter distances during a M6.8 earthquake has shown a trend compatible with a corresponding case history of road embankments.

1 CONCEPT OF ENERGY-BASED NEWMARK METHOD

To evaluate seismic slope failures in terms of energy, an energy approach was previously proposed by the present author (Kokusho & Ishizawa 2007). In that method, earthquake-induced slope displacement δ_r is expressed simply as;

$$\delta_r = E_{eq}/[\rho Dg \tan(\phi - \theta)] \tag{1}$$

where, E_{eq} = earthquake energy for slope sliding in unit area, ρ and D= density and thickness of sliding soil mass, respectively, g=acceleration of gravity, ϕ = mobilized slope friction angle including cohesion effect, and θ = slope angle. This equation was theoretically derived from energy balance in slope failures and demonstrated by model shaking table tests.

As its extension, "Energy-Based Newmark Method" is proposed here wherein the earthquake energy can determine occurrence/nonoccurrence of slope failure and, if it occurs, uniquely calculate slope displacements irrespective of earthquake motions unlike conventional Newmark methods. A slope model is employed as depicted in Figure 1 where an infinitely long slope with an overlying sliding block is shaken underneath by SH-wave. The slope shaded in the figure is virtually of infinite rigidity and no mass and resting on a horizontal layer. In the layer where the vertical z-axis is taken upward from the surface, SH-wave displacements u(t, z), consisting of upward and downward components u_1 and u_2 , propagates at a depth as;

$$u(t,z) = u_1(t - z/V_s) + u_2(t + z/V_s)$$
(2)

Then, surface acceleration of the horizontal layer (z=0) can be expressed as;

$$\ddot{u}(t,0) \equiv \ddot{u}_0(t) = \ddot{u}_1(t) + \ddot{u}_2(t) \tag{3}$$

The earthquake energy E_{eq} for slope sliding can be expressed as the difference of upward and downward wave energies E_u and E_d in the assumption of 1-D SH-wave propagation.

$$E_{eq} = E_u - E_d \tag{4}$$

Here, the wave energies can be calculated from the respective particle velocities $\dot{u}_1(t)$ and $\dot{u}_2(t)$ at the top of horizontal layer as;

$$E_{u} = \rho_{s} V_{s} \int_{0}^{T} [\dot{u}_{1}(t)]^{2} dt, \ E_{d} = \rho_{s} V_{s} \int_{0}^{T} [\dot{u}_{2}(t)]^{2} dt$$
 (5)

In the Newmark model (Newmark 1965), relative acceleration of the block $\ddot{\delta}_r(t)$ sliding down-slope is expressed as (Sarma 1975);

$$\ddot{\delta}_r(t) = [\ddot{u}_0(t) - g\tan(\phi - \theta)]\cos(\phi - \theta)\cos\theta/\cos\phi \tag{6}$$

where ϕ =friction angle between the block and slope and θ = slope angle. In Eq. (6), $\ddot{\delta}_r$ >0 only if $\ddot{u}_0(t)$ the exceeds a threshold acceleration defined as;

$$\ddot{u}_0 = g \tan(\phi - \theta) \tag{7}$$

Horizontal force equilibrium of the block coupled with the SH-wave vibration transmitted through the virtual slope body can be expressed as;

$$\rho D(\ddot{u}_0(t) - \ddot{\delta}_r(t)) + G_s(\partial u(t, z)/\partial u)|_{z=0} = 0$$
(8)

where $\ddot{u}_0(t) - \ddot{\delta}_r(t)$ is absolute acceleration of the block, and $G_s = \rho_s V_s^2$ is shear stiffness of the soil layer. Substituting Eq. (2) into Eq. (8) yields the following key equation.

$$\rho D(\ddot{u}_1(t) + \ddot{u}_2(t) - \ddot{\delta}_r(t)) = \rho_s V_s [\dot{u}_1(t) - \dot{u}_2(t)] \tag{9}$$

Eq. (9) together with Eq. (6) can solve the slope system shown in Figure 1. Its stationary harmonic response for angular frequency ω can be obtained by substituting

$$\ddot{u}_1(t) = A_1 e^{i\omega t}, \\ \ddot{u}_2(t) = A_2 e^{i\omega t}, \\ \dot{u}_1(t) = (A_1/i\omega)e^{i\omega t}, \\ \dot{u}_2(t) = (A_2/i\omega)e^{i\omega t}$$
(10)

into Eqs. (9) as;

$$i\frac{\omega\rho D}{\rho_s V_s} \left[(A_1 + A_2)e^{i\omega t} - \ddot{\delta}_r(t) \right] = (A_1 - A_2)e^{i\omega t} \tag{11}$$

Obviously, $\alpha = \omega \rho D/(\rho_s V_s)$ serves as a governing parameter in Eqs. (11) and (9), and named as a block impedance ratio α , wherein $\omega \rho D$ has the same dimension as $\rho_s V_s$. The nonlinear equations Eqs. (9) and (6) for $\ddot{\delta}_r(t)\neq 0$ has to be solved by a numerical method as explained below.

2 NUMERICAL ANALYSIS

Time integration of Eq. (9) together with Eq. (6) was implemented for a given input harmonic motion by using Wilson's "Theta-method" with "Theta" =1.4 to have a stable solution. Figure 2 exemplifies the numerical results of a slope of ϕ =35°, θ =30°, D=10 m, V_s =200 m/s, and $\rho = \rho_s = 1.8$ t/m³. As the input wave, a 10-cycle harmonic wave of frequency f=1.0 Hz was given wherein the amplitude was tapered from 0 to 100% linearly with time in the former 5 cycles to avoid unfavorable effects of initial conditions followed by a 100% constant amplitude (A_1 =2.0 m/s²) in the latter 5 cycles. The slope starts to slide at 2nd cycle when \ddot{u}_0 exceeds a threshold (0.85 m/s²) defined by Eq. (7), and accumulates downslope displacements δ_r .

The bottom frame of Figure 2 shows time-dependent variations of the associated energies. As the difference of energy $E_{eq}=E_u-E_d$ accumulates with time, its sum with the gravitational energy $E_{eq}+E_{gr}$ is observed to be identical with the energy dissipated by the friction between

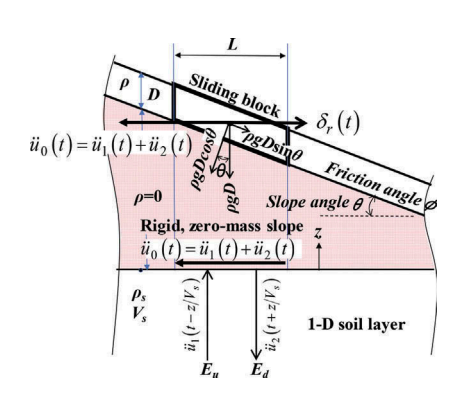


Figure 1. Infinitely long slope model with SH-wave propagated underneath employed in Energy-Based Newmark Method.

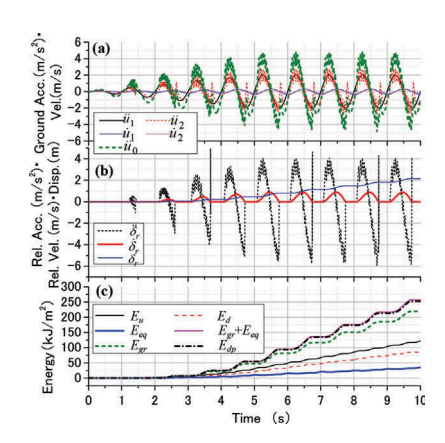


Figure 2. Exemplified analytical result of Energy-Based Newmark slope model by a tapered harmonic input wave (ϕ =35°. θ =30°).

the block and slope E_{ds} . This exactly satisfies the energy balance already discussed theoretically in previous papers and demonstrated in previous model tests (e. g. Kokusho 2017).

Figure 3 (a) shows a slope displacement δ_r versus earthquake energy E_{eq} relationship calculated as a stationary response per one cycle (in the 10^{th} cycle of the tapered harmonic wave for various input accelerations). The calculations conducted for 3 different frequencies f=0.5~1.0 Hz tend to give a unique correlation for the displacement δ_r around 0.3 m or smaller though they tend to diverge with increasing δ_r for higher f in particular presumably due to errors in the numerical analysis. Also note that for the small displacements the calculated results coincide with dashed straight line in the diagram representing Eq. (1) derived theoretically from a simple energy principle (Kokusho & Ishizawa 2007). In Figure 3 (b), the same calculated δ_r -values are plotted versus amplitude (A_1) nearly a half of slope acceleration quite differently for different f-values, indicating that not the acceleration but the energy can serve as a unique indicator for slope displacements as already observed in previous model tests (Kokusho & Ishizawa 2007).

A series of analyses conducted for a set of parameters, ϕ =35°, θ =20~30°, f=0.5~1.0Hz, D=2.5~10 m, V_s =150~300 m/s, yield relationships for a given earthquake wave between normalized energies (E_{eq}/E_u)/ α and (E_u/N_{eq})/ E_{u0} superposed in Figure 4, where $\alpha = \omega \rho D/(\rho_s V_s)$ is the block impedance ratio, N_{eq} = equivalent number of cycles and E_{u0} is threshold upward energy initiating slope sliding for an equivalent harmonic motion with its angular frequency $\omega = 2\pi f$.

$$E_{u0} = \frac{\pi \rho_s V_s}{4\omega^3} g^2 \tan^2(\phi - \theta)$$
 (12)

A trilinear dashed line ABCD may be drawn commonly for all the parameters considered here, formulating the following equation despite data dispersions;

$$\frac{(E_u/N_{eq})/E_{u0} < 1.0:}{1.0 < (E_u/N_{eq})/E_{u0} < 5.0:} \frac{(E_{eq}/E_u)/\alpha = 0}{(E_{eq}/E_u)/\alpha = 1.43\log_{10}[(E_u/N_{eq})/E_{u0}]}$$

$$5.0 \le (E_u/N_{eq})/E_{u0}: \frac{(E_{eq}/E_u)/\alpha = 1.0}{(E_{eq}/E_u)/\alpha = 1.0}$$
(13)

In the trilinear line, the section CD ($(E_{eq}/E_u)/\alpha=1.0$) is drawn quite differently from the calculation results because all the plots located on the right side of peaks or plateaus were found less reliable with growing gaps from theoretical values in Eq. (1), and also it is on the safer side. Using the earthquake energy E_{eq} in Eq. (13), the residual slope displacement δ_r can be calculated from Eq. (1) using upward energy E_u depending on the block impedance ratio α and the threshold energy E_{u0} in Eq. (12).

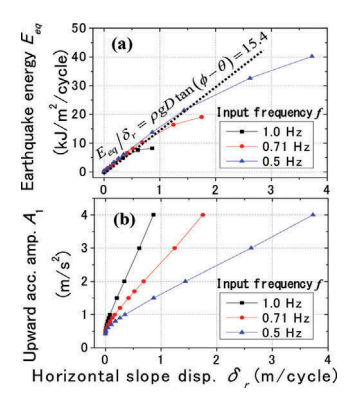


Figure 3. Earthquake energy E_{eq} (a) or upward acceleration amplitude A_1 (b) versus horizontal slope displacement δ_r .

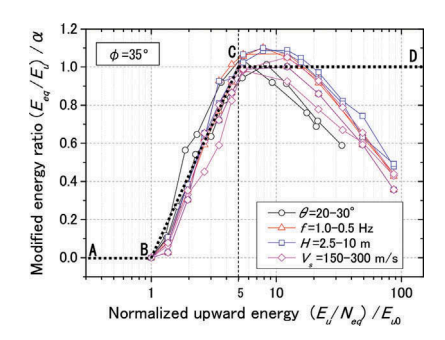


Figure 4. $E_{eq}/E_u/\alpha$ and E_u/E_{u0} relationships obtained by a series of numerical analyses for various parameters and simplified dashed trilinear line.

3 UPWARD WAVE ENERGY EVALUATION

In order to evaluate residual slope displacements δ_r by combining Eqs. (1) and (13), it is essential how to determine upward wave energy per unit horizontal area E_u in actual site conditions. For that goal, empirical formulas on earthquake wave energy employing a number of vertical array strong motion records during recent earthquakes in Japan can be utilized.

Figure 5 summarizes upward energy versus ground depth z correlations calculated in 30 vertical array sites during 9 strong earthquakes EQ.1~EQ.9 of earthquake magnitude M_J = 6.4 to 8.0 (M_J : Japanese Meteorological Agency magnitude similar to moment magnitude M_W) and hypocenter distance R=9~227 km on a semi-log diagram (Kokusho & Suzuki 2012). They were calculated using the first formula in Eq. (5) from upward velocity waves and associated S-wave impedance values. The velocity waves were calculated by a series of one-dimensional equivalent linear soil response analyses conducted for those sites using acceleration records, soil profiles and soil properties (soil density, strain-dependent S-wave velocity and damping ratio). The energies calculated in two orthogonal directions were summed up to have two-directional upward energy, denoted here as $E_{u, \text{2D}}$. The energy tends to decrease drastically with decreasing depth almost monotonically in most sites for all the sites. Details of the calculations are available in two previous literatures (Kokusho & Suzuki 2012).

In order to know more clearly how the upward energy tends to decrease as it approaches to the ground surface, an additional study was carried out wherein the ratio of upward energies between layers is correlated to corresponding S-wave impedance ratio. Out of the 30 sites plotted in Figure 5, 23 sites with higher reliability have been used (Kokusho & Suzuki 2012). The ratio of upward energy $(E_{u,2D})_i/(E_{u,2D})_{i+1}$ between two arbitrary neighboring layers, i (upper) and i+1 (lower) from the surface to the base layer of vertical array sites, are plotted versus corresponding impedance ratio $(\rho_s V_s)_i/(\rho_s V_s)_{i+1}$ in Figure 6(a) for all layers above the deepest levels in vertical array sites with different symbols. For the majority of the data points where $(\rho_s V_s)_i/(\rho_s V_s)_{i+1} < 1.0$ because the impedance ratio is normally less than unity, it is quite reasonable to postulate that $(E_{u,2D})_i/(E_{u,2D})_{i+1}=0$ for $(\rho_s V_s)_i/(\rho_s V_s)_{i+1}=0$ (free surface), and $(E_{u,2D})_i/(E_{u,2D})_{i+1}=1$ for $(\rho_s V_s)_i/(\rho_s V_s)_{i+1}=1$ (a uniform layer without a property boundary). Hence, a simple power function as follows may be used to approximate the plots and the power 0.70 can be obtained from the least mean-square method with the determination coefficient $R^2=0.81$.

$$(E_{u,2D})_i/(E_{u,2D})_{i+1} = [(\rho_s V_s)_i/(\rho_s V_s)_{i+1}]^{0.70}$$
 (14)

Thus, the thick solid curve of Eq. (14) shown in the Figure 6 (a) approximates the data points fairly well up to $(\rho V_s)_i/(\rho V_s)_{i+1}=1.0$. Figure 6 (b) shows a similar diagram to (a), but the

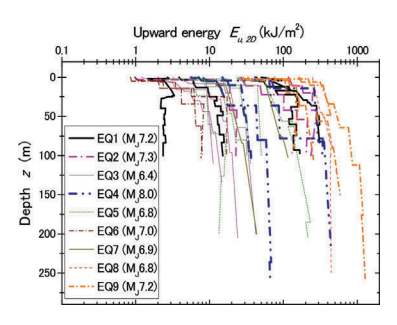


Figure 5. Upward energy $E_{u,2D}$ versus depth z in 30 vertical array sites during 9 strong earthquakes.

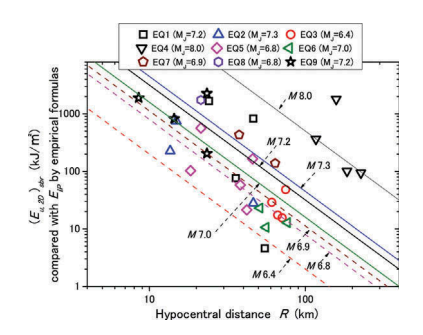


Figure 7. Upward energy $E_{u,2D}$ versus hypocentral distance R at seismological bedrock compared with incident energy E_{IP} during 9 earthquakes.

2400 \Vs

1.0 1.2

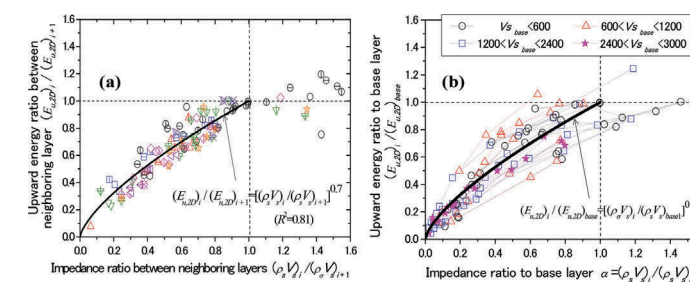


Figure 6. Upward energy ratio versus impedance ratio based on vertical array strong motion records:

- (a) $(E_{u,2D})_i/(E_u)_{i+1}$ and $(\rho_s V_s)_i/(\rho_s V_s)_{i+1}$ between neighboring layers,
- (b) $(E_{u,2D})_i/(E_u)_{base}$ and $(\rho_s V_s)_i/(\rho_s V_s)_{base}$ between i^{th} and base layer.

upward energy ratio and the impedance ratio there are redefined between an arbitrary layer i and the base layer (the deepest layer of vertical arrays) as $(E_{u,2D})/(E_{u,2D})_{base}$ and $(\rho V_s)/(\rho V_s)_{base}$. respectively. In this chart, symbols belonging to the same sites are connected with dashed lines and differentiated according to 4 classes of V_s -values at the base layer. The curve superposed here is the similar function of the same power 0.70;

$$(E_{u,2D})/(E_{u,2D})_{base} = [(\rho_s V_s)/(\rho_s V_s)_{base}]^{0.70}$$
 (15)

and seems to averagely represent the plots. Among the plots, the star symbols representing those sites for 2400 m/s $< V_s <$ 3000 m/s (almost as stiff as seismological bedrock) fit well with the curve near the origin (at smaller α -values) in particular. This indicates that it may be possible to use Eq. (15) to evaluate the upward energy in a soil layer near the ground surface from the upward energy at a rock base almost as stiff as seismological bedrock by considering the impedance ratio between the two corresponding layers. Further details of the research are available in Kokusho & Suzuki (2012). Hence, Eq. (15) may be modified to estimate the upward energies at the seismological bedrock $(E_{u,2D})_{sbr}$ from those at the base layers of vertical arrays $(E_{u,2D})_{base}$ as;

$$(E_{u,2D})_{base}/(E_{u,2D})_{sbr} = [(\rho_s V_s)_{base}/(\rho_s V_s)_{sbr}]^{0.70}$$
 (16)

if the vertical propagation of SH wave is postulated down there by ignoring slanting wave effects. As normally accepted in engineering seismology, the impedance for the seismological bedrock is assumed as $(\rho_s V_s)_{sbr}$ =2.7 t/m³×3000 m/s for all the vertical array sites.

Figure 7 shows the energies $(E_{u,2D})_{sbr}$ thus calculated at seismological bedrocks in Eq. (16) and plotted versus corresponding hypocentral distances R. Straight diagonal lines drawn in

the chart represent incident energy E_{IP} calculated for the individual earthquakes from the following empirical formulas sometimes employed in previous researches (e.g. Sarma 1970, Davis and Berrill 1982) based on spherical energy radiation of body waves using the earthquake magnitude M and the distance from the center of energy release R.

$$E_{IP} = E_{total}/(4\pi R^2), \quad log E_{total} = 1.5M + 1.8$$
 (17)

Here, E_{IP} is in kJ/m², R in m, and E_{total} is the total energy released from fault in kJ proposed by Gutenberg (1956). M_J is used here for M and the distance R is approximated by the hypocentral distance.

The energy predictions by Eq. (17) are far from perfect because they completely neglect pertinent fault and path parameters, such as fault type, fault size/depth, asperity, directivity, etc. However, decreasing trends of $E_{u,2D}$ with increasing R for individual earthquakes may be recognizable despite data dispersions. The paramount effect of earthquake magnitude can also be seen, as the plots of EQ4 of $M_J = 8.0$ among the 9 earthquakes are located relatively higher on the right side of the diagram, while others of $M_J \approx 7$ are lower on the left side. Though, more detailed study is certainly needed to consider the source and path effects on the $E_{u,2D}$ versus R correlations, Eq. (17) is used at this moment to determine the incident energy E_{IP} at the seismological bedrock of a given site for the energy-based slope displacement evaluation.

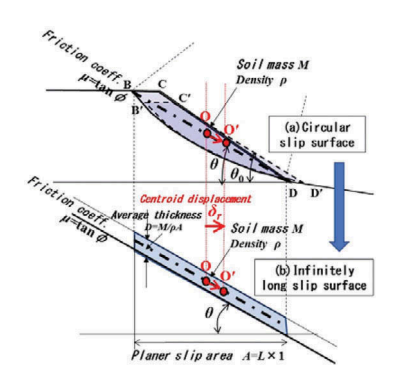
Upward energy $E_{u,2D}$ summed up in two horizontal orthogonal directions at a slope can be evaluated by substituting $(E_{u,2D})_{base} = E_{IP}$ and $(\rho_s V_s)_{base} = 1.8 \text{ t/m}^3 \times 3000 \text{ m/s}$ into Eq. (15). The upward energy E_u in a sloping direction is calculated as $E_u = E_{u,2D}/2$ based on previous research finding by earthquake observations that the two-directional upward energy $E_{u,2D}$ is evenly distributed in two orthogonal directions on average (Kokusho et al. 2014).

4 SLOPE DISPLACEMENT EVALUATION EXAMPLE

Figure 8 (a) exemplifies a typical slope profile for conventional Newmark-type slope analysis along a circular slip surface, wherein the centroid O of soil block BCD slides to O' of B' C' D'. If the sliding displacement is not so large (less than a few meters for normal engineering problem) relative to slope length, the line OO' may be approximated being parallel to the line BD with its angle θ . Hence, it may be replaced in the energy method by a slide of an infinitely long slope with the same horizontal length L and angle θ as depicted in Figure 8 (b), wherein the mass M and planar slip area $A=L\times 1$ are the same (exposed to the same upward wave energy) and the sliding soil thickness $D=M/(\rho A)$. If it is assumed that the angles of BD and CD with respect to the horizontal plane $\theta=30^{\circ}$, $\theta_0=35^{\circ}$, respectively, the radius of circular slip surface R=50 m, and L=34.7 m, the cross-sectional area (shaded in the figure) is calculated as a=174 m², and the average sliding block thickness becomes D=a/L=174/34.7=5.0 m.

Alternatively, the energy method may also be implemented directly using the infinitely-long slope model for the purpose of screening potentially instable slopes in a wide area with no specific failed slope size converted from conventional slip-surface models.

If the slope in Figure 8 undergoes an earthquake of the magnitude M=6.8 such as the 2004 Niigataken Chuetsu earthquake, the upward wave energy beneath the slope in the downslope direction E_u is calculated following the steps shown in Figure 9 (a) using Eq. (15) as E_u = $E_{u,2D}$ /2= 45.0~2.81 kJ/m² from the incident energy at a bedrock as $(E_{u,2D})_{base}$ = E_{IP} =796~49.7 kJ/m² using Eq. (17) for R=10~40 km. Then, the irregular earthquake wave having the upward energy E_u is converted to an equivalent harmonic acceleration wave $\ddot{u}_1(t) = A_1 \sin \omega t$ as Figure 9 (b), with the amplitude A_1 , the angular frequency $\omega = 2\pi f$, and the equivalent number of cycles N_{eq} , so as to have the same energy E_u as the irregular wave. The number of cycles for the earthquake may be determined as N_{eq} =9 from M=6.8 based on empirical relationships, e.g. by Idriss & Boulanger (2008). The amplitude A_1 may be determined from PGA given by empirical attenuation formulas and the amplitude reduction coefficient 0.65 frequently used in soil dynamics as A_1 =0.65×(1/2) ×PGA, where the coefficient 1/2 reflects that PGA is defined at a free ground surface. PGA attenuation data for the same 2004 earthquake



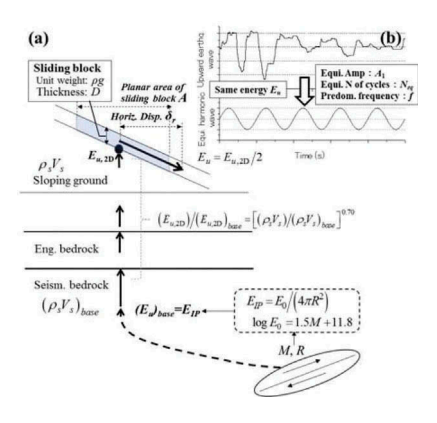


Figure 8. Slope failures along circular surface (a) and straight surface (b) having the same soil mass and planer area.

Figure 9. Evaluation steps for upward earthquake wave energy E_u (a), and conversion of irregular wave to equivalent harmonic wave of same energy (b).

(NIED 2004) may be approximated to be inversely proportional to the fault distance R (km) approximated here by hypocentral distance as $PGA(\text{m/s}^2)=6.0\times(R^*/10\text{ km})^{-1}$ for the range of $R^*=10\sim100$ km. The acceleration amplitude of equivalent harmonic wave $A_1=1.95\sim0.49\text{ m/s}^2$ can be obtained from $PGA=6.0\sim1.5\text{ m/s}^2$ for $R=10\sim40$ km. These A_1 -values yield $f=\omega/2\pi=1.51$ Hz commonly to have the same wave energy E_u by using Eq. (5).

Then, the upward energy per cycle $E_u/N_{eq}=5.00\sim0.313$ kJ/m² for $R=10\sim40$ km is compared with the threshold energy E_{u0} calculated in Eq. (12) for various $\phi-\theta$ to obtain energy ratio $(E_u/N_{eq})/E_{u0}$, and the energy E_{eq} can be determined in Eq. (13) from E_u and the block impedance ratio $\alpha=\omega\rho D/(\rho_s V_s)$. Finally, the sliding displacement δ_r can be obtained from Eq. (1).

The displacements δ_r thus calculated in the above-mentioned steps are plotted with solid symbols in Figure 10 (a) versus the angular difference $\phi - \theta$ with the pitch of 1°. The open symbols correspond to the bottom formula of Eq. (13) $E_{eq}/E_u/\alpha=1.0$ without being controlled by the parameter $(E_u/N_{eq})/E_{u0}$. The displacement δ_r follows these open plots for $(E_u/N_{eq})/E_{u0}$ 5, and separates from them downward decreasing more rapidly corresponding to the middle formula of Eq. (13) for $5>(E_u/N_{eq})/E_{u0}>1$, and reach $\delta_r=0$ corresponding to the top formula of Eq. (13) if $(E_u/N_{eq})/E_{u0} \le 1$. Thus, this method can cover the variations of slope displacement including zero (no-sliding) depending on the angular difference $\phi - \theta$ for different hypocenter distance R as a parameter. Though Figure 10 (a) is for a particular case of M=6.8, analogous charts of different cases can be readily made using Eq. (13) which is universally applicable to varying parameters.

In Figure 10 (b), the top diagram shows the same calculated displacements δ_r plotted versus hypocentral distance R with the value $\phi - \theta$ as a parameter. To compare with this, the bottom diagram shows hypocentral distances R of embankments of Kan-etsu high-speed roadway damaged during the same 2004 earthquake reported by Kataoka et al. (2015). The same authors classified the damage into A (heavy), B (medium), C (light), corresponding to

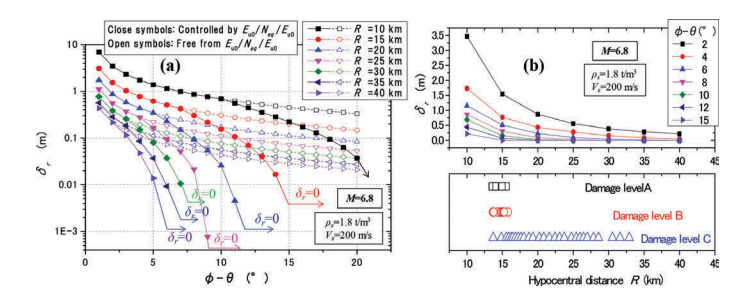


Figure 10. Example evaluation of embankment slope displacements by M=6.8 earthquake: (a) displacements δ_r versus θ -0 for varying hypocenter distance R, (b) δ_r versus R compared with case history data.

embankment displacements of larger than 50 cm, 50~30 cm and smaller than 15 cm, respectively. The sections of Class A and B are similarly located in the hypocentral distance $R=13\sim16$ km and possible combinations of δ_r and $\phi-\theta$ can be read off from the top chart. For Class C (the light damage), the longest R-value is 33 km in the bottom chart, and if this distance is interpreted as a boundary of zero slope displacement, the top chart indicates that $\phi-\theta=6^\circ$ seems to be able to explain the performance of embankments in the conditions assumed here.

Finally, note that the sliding block thickness D, an important parameter to determine the displacement $\delta_r = E_{eq}/[\rho Dg\tan(\phi-\theta)]$ from E_{eq} in Eq. (1), is eventually eliminated together with the density ρ when δ_r is correlated to E_u in place of E_{eq} , because E_{eq} is proportional to αE_u in Eq. (13) where $\alpha = \omega \rho D/(\rho_s V_s)$, though D has been used in the above example as an intermediate parameter. The absence of D in determining δ_r from E_u seems to be beneficial in applying this method to various site conditions in general. In return to that, the thickness D together with length L of the failure block has to be determined in individual sites considering site-specific slope profiles and cross-sectional spatial variations of friction angle ϕ by consulting with a chart as exemplified in Figure 10. In addition, an upper limit of D is imposed as $D < (\lambda/4\pi)(\rho_s/\rho) \approx \lambda/4\pi$. It is because with regard to the maximum energy ratio $E_{eq}/E_u = \alpha = \omega \rho D/(\rho_s V_s)$ in Eq. (13), E_u includes the energy in both downslope and upslope directions while the energy E_{eq} contributing solely to downslope slide cannot be larger than 1/2 of E_u on average, as actually confirmed by earthquake observation data (Kokusho et al. 2014).

5 SUMMARY

Energy-based Newmark method has been developed based on a series of nonlinear numerical analyses where Newmark-type slope model is shaken by SH-wave propagation underneath. Occurrence/Nonoccurrence of slope failures as well as associated slope displacements can be evaluated directly from upward wave energy using pertinent slope parameters with no need of acceleration time histories. An example study by this method wherein pertinent parameters with uncertainties such as friction angle ϕ and earthquake energy E_{eq} are continuously varied has indicated a qualitative compatibility with a case history of embankment failures during a M6.8 earthquake in Japan. Though more case studies are certainly needed to demonstrate its higher reliability in employing it in engineering design, the present study has indicated that the energy-based Newmark method developed here is quite convenient to seamlessly evaluate slope displacements using design charts as exemplified in Figure 10.

REFERENCES

Gutenberg, B. (1956): The energy of earthquakes, *Quarterly Journal of the Geological Society of London*, Vol. CXII, No.455, 1–14.

Idriss, I.M. and Boulanger, R. (2008): Soil liquefaction during earthquakes, *Earthquake Engineering Research Institute*, MNO-12, p.92.

Kataoka, S., Nagaya, K. and Matsumoto, K. (2015). Analysis on damage to road embankments caused by the Mid Niigata Prefecture earthquake 2004, *Journal of Japan Society for Civil Engineers*, JSCE Vol. 71(4),568–576.

Kokusho, T. and Ishizawa, T. (2007). Energy approach to earthquake-induced slope failures and its implications, *Journal of Geotechnical and Geoenvironmental Engineering*, ASCE Vol.133, No.7, 828–840.

Kokusho, T. and Suzuki, T. (2012). Energy flow in shallow depth based on vertical array records during recent strong earthquakes (Supplement), Soil Dynamics & Earthquake Engineering, Vol. 42, 138–142.

Kokusho, T., Koyanagi, T. and Yamada, T. (2014). Energy ap proach to seismically induced slope failure and its application to case histories –Supplement-, *Engineering Geology*, Elsevier, Vol. 181, 290–296.

Kokusho, T. (2017). Innovative Earthquake Soil Dynamics, Chap.4, CRC publishers. P9.

Newmark, N. M. (1965). Effects of earthquakes on dams and embankments, Fifth Rankine Lecture, Geotechnique Vol.15, 139–159.

NIED: 2004 Niigataken Chuetsu earthquake; motion and fault http://cais.gsi.go.jp/KAIHOU/report/kaihou73/07 16.pdf

Sarma, S. K. (1975). Seismic stability of earth dams and embankments, Geotechnique, 25, No.4, 743-761.